CTRC Research Publications   Cooling Technologies Research Center

2004

Thermal Management of Transient Power Spikes in Electronics - Phase Change Energy Storage or Copper Heat Sinks?

S. Krishnan

S V. Garimella
Purdue University, sureshg@purdue.edu

Thermal Management of Transient Power Spikes in Electronics—Phase Change Energy Storage or Copper Heat Sinks?

Shankar Krishnan

Suresh V. Garimella
e-mail: sureshg@ecn.purdue.edu

Cooling Technologies Research Center,
Purdue University,
West Lafayette, Indiana 47907-2088

A transient thermal analysis is performed to investigate thermal control of power semiconductors using phase change materials, and to compare the performance of this approach to that of copper heat sinks. Both the melting of the phase change material under a transient power spike input, as well as the resolidification process, are considered. Phase change materials of different kinds (paraffin waxes and metallic alloys) are considered, with and without the use of thermal conductivity enhancers. Simple expressions for the melt depth, melting time and temperature distribution are presented in terms of the dimensions of the heat sink and the thermophysical properties of the phase change material, to aid in the design of passive thermal control systems. The simplified analytical expressions are verified against numerical simulations, and are shown to be excellent tools for design calculations. The suppression of junction temperatures achieved by the use of phase change materials when compared to the performance with copper heat sinks is illustrated. Merits of employing phase change materials for pulsed power electronics cooling applications are discussed. [DOI: 10.1115/1.1772411]

Introduction

Phase change thermal energy storage is one of three available ways to store heat, the other two methods being sensible heat energy storage and chemical energy storage. In phase change thermal energy storage, heat is stored by exploiting the latent heat of phase change of the medium. The temperature of the phase change material (PCM) remains more or less constant during this phase transformation. Solid-liquid phase change thermal energy storage has been used in a wide range of applications including solar energy and aerospace thermal management.

Thermal transients occur in power semiconductors and electronics due to the current in-rush while starting a motor, in inductive devices such as heaters and transformers, in capacitive charging, and in power grid management. The suppression of temperature overshoots during the dissipation of transient power spikes is an important challenge in electronics package design. The maximum temperature allowable for most electronics is typically 100-120°C. The general approach for managing these transient spikes has been to use solid copper heat sinks to absorb the thermal transients. Use of a PCM storage unit as an alternative to the copper heat sinks has the potential to lower junction temperatures [1,2], while at the same time yielding weight and volume savings. Since the thermal transients in many applications last only for short periods, the PCM has a chance to recharge (solidify) between pulses.

The present work considers the thermal performance of a phase change energy storage unit with and without thermal conductivity enhancers (porous metal foams) included. The problem considered is melting and resolidification of a phase change material inside a rectangular enclosure. A set of exact and approximate expressions are developed for use in designing PCM storage units. The formulas developed cover transient heating and cooling of a finite slab of material without phase change (as applicable to solid copper heat sinks), as well as melting and resolidification of a PCM inside rectangular enclosures. The validity of the approximate expressions developed is also discussed, by comparison against more rigorous numerical simulations. In a series of calculations, the thermal performance of a PCM energy storage unit is compared to that of a solid copper heat sink to illustrate the design process.

Mathematical and Numerical Analysis

A schematic of the problem being considered is shown in Fig. 1. The height (H) and thickness (L) of the domain were assumed to be 70 mm and 10 mm, respectively, to simulate a typical power semiconductor unit. (The third dimension, typically on the order of 140 mm, is not considered in this two-dimensional study, except in calculating input heat flux over a cross-sectional area A of 70 mm by 140 mm.) One of two different heat input pulses was applied on the left wall, either 600 W for 25 s or 300 W for 50 s, corresponding to different possible startup conditions for motor drives depending on the in-rush current drawn by the motor. The top and bottom walls were considered to be adiabatic as a worst-case test of the thermal management unit. A uniform heat transfer coefficient of 12 W/m² °C with an ambient temperature of 40°C were specified on the right wall.

The thermophysical properties of the materials used are listed in Table 1 [3–5], and are assumed to remain constant over the range of temperatures considered. The properties listed for the PCMs are averaged over liquid and solid phases. The volume change of the PCM ($\rho_l = \rho_s$) during melting is neglected in this work. Since the problem is essentially conduction-dominated (natural convection in the melt being negligible owing to the small thickness L), the governing equation for energy transport [6,7] in the domain is:

$$\rho C_p \frac{\partial T}{\partial t} = \bar{\nabla} \cdot (k \bar{\nabla} T) - \rho ([C_{pl} - C_{ps}] T + \Delta H) \frac{\partial f_l}{\partial t} \qquad (1)$$
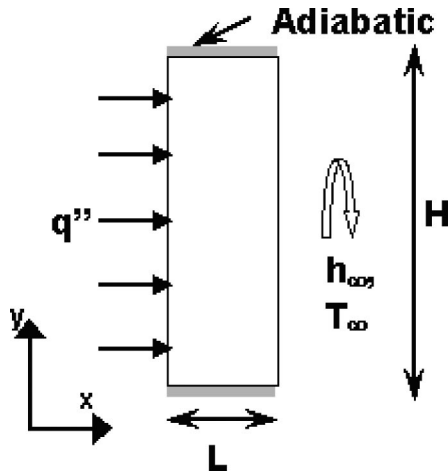
Fig. 1 Schematic diagram of the problem considered

Fig. 2 Interface locations as a function of time for different Stefan numbers

The governing equations are solved using a finite-volume technique on orthogonal, fixed grids. A central differencing scheme is used for the diffusive fluxes and a three time-level scheme (2nd order Euler) is used for the transient terms [8]. Since numerical algorithms have difficulty in handling step-functions, the fraction of liquid and temperature are smoothed [7,9] according to:

$$f_l = \begin{cases} 0 & T_p < (T_{melt} - \eta) \\ \dfrac{T_p - T_{melt} + \eta}{2\eta} & (T_{melt} - \eta) \leqslant T_p \leqslant (T_{melt} + \eta) \\ 1 & T_p > (T_{melt} + \eta) \end{cases} \quad (2)$$

The solution of the energy equation is insensitive to the assumed variation of f_l with temperature if η is relatively small. For the computations performed in this study, η_{max} was 0.1°C, which ensures that a temperature change of 2η occurs within a single computational control volume at any given time step. Further details of the solution procedure and discretization are available in [6,7].

Code Validation. Explicit exact analytical solutions are available for the two-phase Stefan problem [10] against which the code was validated. The problem is one of the melting of a semi-infinite slab initially at a uniform temperature ($T_{initial} \leqslant T_{melt}$). At a given instant, the temperature at $x = 0$ is raised to a temperature $T_H > T_{melt}$. The interface location is given by the relation

$$S(t) = 2\lambda \sqrt{\alpha t}, \quad t > 0$$

which λ is the positive root of the transcendental equation

$$\lambda e^{\lambda^2} \mathrm{erf}(\lambda) = \frac{\mathrm{Ste}}{\sqrt{\pi}} \quad (3)$$

Figure 2 shows a comparison of the predicted interface locations with the analytical predictions as a function of time, for Stefan numbers of 0.1 and 2.85 (corresponding λ values of 0.22 and 0.9). The numerical code developed for analyzing phase change thermal energy storage in the absence of a metal foam has been previously validated and extensively benchmarked by the authors' group [6,7].

A grid-independence study was carried out to test the sensitivity of the chosen grids. Three grids −14×42, 26×82 and 52×162-were tested, and the maximum temperature change was 2.5% between the first two, and 0.4% between the 26×82 and 52×162 grid cases. The 26×82 grid was used for all the computations in this work.

Exact and Approximate Solutions for Conduction and Phase Change

Available analytical solutions for different conduction-based problems are collected in Table 2 [10–13] for use in predictions of the performance of the alternative thermal management options being considered. The junction temperature described in Table 2 is the surface temperature at $x = 0$ at all times. The quasi-stationary approximation assumes that the melting temperature of the domain is the initial temperature and thus, only the solution for the liquid phase is obtained. Hence the influence of the convective boundary condition (right wall) cannot be seen in the listed equations. The quasi-stationary approximation is strictly valid when Ste=0. Since the initial temperature is not equal to the melting temperature in the present work, the time term needs to be adjusted in the equations: assuming the lumped capacitance method to be valid, an approximate time for the PCM to heat up to the melting temperature can be derived by linearising equation (T2) in Table 2 as:

Table 1 Thermophysical properties of materials used [3,4,5]

Property	Copper	Bi/Pb/ Sn/In	Bi/In/ Sn£	Tria-contane	Porous foam with triacontane⊥
Density (kg/m³)	8933	8640	8060.7	810	
Thermal cond. (W/mK)	401	21.9	42.5	0.23	19.7
Specific heat (kJ/kg K)	0.385	0.522	0.203	2.05	1814.4#
Melting temp. (°C)	-	57	60	65	65
Latent heat (kJ/kg)	-	29.5	29.5	251	251

£-Property values not available; weighted-average values for the respective elements used
⊥-Effective properties
#-Thermal capacitance (Eq. (6))

Table 2 Exact and approximate solutions for conduction and phase change processes [10,11,12,13]

Heat Transfer Process (Fig. 1)		Solution	Remarks
Conduction in a Slab (heat input on one side; convection on the other)	Exact (T1)	$$\frac{T(x,t)-T_{\text{initial}}}{q''}=\frac{L-x}{k}+\frac{L}{k}\left\{\frac{1}{\text{Bi}}-2\sum_{n=1}^{\infty}\frac{\exp\left(\frac{-\lambda_n^2 kt}{L^2}\right)\cos\left(\frac{\lambda_n x}{L}\right)}{\lambda_n(\lambda_n+\sin\lambda_n\cos\lambda_n)}\right\},$$ where $\lambda_n\tan\lambda_n=\text{Bi}$	Approximate solution applies if lumped analysis valid (Bi≪0.1)
	Approximate (T2)	$T(t)-T_\infty/(q''/h_\infty)=1-\exp(-\text{Bi}\cdot\text{Fo})$	
Conduction in a Slab -(insulated on one side, convective cooling on the other)	Exact (T3)	$$\frac{T(x,t)-T_\infty}{T_{\text{initial}}-T_\infty}=\sum_{n=1}^{\infty}C_n\exp(-\lambda_n^2\text{Fo})\cos\left(\lambda_n\left(\frac{x}{L}\right)\right),$$ with $C_n=\dfrac{4\sin\lambda_n}{2\lambda_n+\sin(2\lambda_n)}$	
	Approximate (T4)	$$\frac{T(t)-T_\infty}{T_{\text{initial}}-T_\infty}=\exp\left(-\frac{h_\infty}{\rho C_p L}t\right)$$	
Melting (heat input on one side; convection on the other)	Approximate (T5)	$$T_{\text{junction}}(t)=T_{\text{melt}}+\frac{q''}{k_{\text{liq}}}\left\{\frac{q''}{\rho\Delta H}t^*\right\},\quad t_{\text{melt}}=\frac{\rho\Delta H}{q''}L,$$ $$S(t)=\frac{q''t^*}{\rho\Delta H},t^*=t-t_m,$$ $$t_m=\frac{(T_{\text{melt}}-T_\infty)}{q''}(\rho C_p L)$$	*Quasi-stationary approach* used assumes sensible heat negligible compared to latent heat (Ste≈0); method always overestimates solution.
Melting in Porous Foam (heat input on one side; convection on the other)	Approximate (T6)	$$T_{\text{junction}}(t)=T_{\text{melt}}+\frac{q''}{k_{\text{liq}}}\left\{\frac{q''}{\varepsilon\rho\Delta H}(t-t_m)\right\},$$ $$t_{\text{melt}}=\frac{\rho\Delta H\varepsilon V}{Q}$$	Assumes that all the heat supplied goes towards melting
Freezing (insulated on one side, convective cooling on the other)	Approximate (T7)	$$t_{\text{solidification}}=\frac{L^2}{2\alpha_s\text{Ste}_s}\left\{1+\frac{2}{\text{Bi}}+0.25(\text{Ste}_s)\right\},$$ $$t_{\text{solidification}}^{qs}=\frac{L^2}{2\alpha_s(\text{Ste})_s}\left\{1+\frac{2}{\text{Bi}}\right\}$$ for $0\leq\text{Ste}_s\leq4,\text{Bi}\geq0.1$	Second expression valid only if $$\text{Bi}<\frac{2}{(\text{Ste}/2\lambda^2-1)},$$ with $$\lambda e^{\lambda^2}\text{erf}(\lambda)=\frac{\text{Ste}}{\sqrt{\pi}}$$

$$T(t)-T_\infty=(q''/h_\infty)\left(1-\exp\left(-\frac{h_\infty t}{\rho C_p L}\right)\right)\approx(q''/h_\infty)\left(\frac{h_\infty t}{\rho C_p L}\right)$$

so that

$$t_m=\frac{(T_{\text{melt}}-T_\infty)}{q''}(\rho C_p L) \tag{4}$$

This expression (4) may also be obtained from an energy balance ($q''t=\rho C_p\Delta TL$). The time in the calculation of quasi-stationary temperatures is corrected using equation (4), and the corrected time appears as $t^*(=t-t_m)$ in the equations listed in Table 2.

For use with the expressions for melting/re-solidification in Table 2, an effective Stefan number can be defined [10] for the problem under consideration as:

$$(\text{Ste})_{\text{eff}}=\frac{Q}{\rho\Delta H\alpha}=\frac{C_p Q}{k\Delta H}$$

The heat transfer rate Q in the above expression has units of W/m with the length scale being A/L. This is an alternate definition for Stefan number, and the magnitude cannot be directly compared to values from the standard definition ($\text{Ste}=C_p\Delta T/\Delta H$). For higher values of Stefan number defined in this manner, the quasi-

stationary approach fails (triacontane being an example), as can be seen in Table 3, in which the predicted temperatures from the rigorous numerical analysis are compared with those obtained from the quasi-stationary approximation. The approximate equations are seen to compare well with the numerically predicted values for the materials considered. For the copper heat sinks, the lumped capacitance method was used.

By recasting equation (T5) suitably, a thermal resistance for the PCM unit can be defined:

$$\frac{T(t)-T_{\text{melt}}}{Q}=\frac{L}{kA}\frac{Qt^*}{(\rho\Delta HV)}=\frac{L}{kA}\frac{E_{\text{in}}}{E_{\text{stored}}} \tag{5}$$

From this expression, it can be seen that thermal resistance for the PCM is a product of conduction resistance and the ratio of heat energy input to the maximum available latent heat energy. The cross-sectional area A in this expression is assumed in all the results shown to be 70 mm (height) by 140 mm (depth). The thermal resistances of the various materials considered in this work are shown as a function of time in Fig. 3. In this figure, it is assumed that the phase change material is at the melting tempera-

Table 3 Comparison of numerically predicted and approximate junction temperatures (°C) for the 300 W-50 s (top) and 600 W-25 s (bottom) pulses

Material	Junction Temperature, Numerical	Junction Temperature, Eq. (T5)
Copper	84.3	84.1^
Bi/Pb/Sn/In	60.9	61.1
Bi/Sn/In	63.4	63.6
Triacontane#	359.3	882.2
Porous Foam	72.9	73.7

Material	Junction Temperature, Numerical	Junction Temperature, Eq. (T5)
Copper	84.7	84.3^
Bi/Pb/Sn/In	64.6	65.4
Bi/Sn/In	66.8	67.2
Triacontane#	438.3	1699.5
Porous Foam	79.9	82.0

#-Quasi-stationary approximation fails due to very high Stefan number.
^-From Eq. (T1)

Fig. 4 Junction temperature as a function of time in the copper heat sink

ture at $t=0$ (i.e. $t_m=0$). It is clear from the figure that the metallic eutectic alloys would perform better than the triacontane or the solid copper block.

Results and Discussion

Solid Copper Block. Results for a solid copper heat sink are shown in Fig. 4 in terms of predicted junction temperatures at the mid-height ($y=35$ mm) as a function of time; solutions from both a detailed numerical analysis as well as a simplified, lumped capacitance analysis are shown. The lumped capacitance approximation is seen to yield results that agree very well with those from the more rigorous numerical analysis. Since the junction temperature is an exponential function of the product of Biot and Fourier

numbers (Eq. (T2)), as this product decreases, the junction temperature approaches the ambient temperature. The Biot number for the copper heat sink is 3×10^{-4} ($\ll 0.1$).

In Fig. 5, the cooling of the copper heat sink after exposure to the 600 W input pulse for 25 s is shown. The predicted junction temperatures are seen to agree very well with those calculated using the lumped capacitance method. The copper heat sink took approximately 37 minutes to cool down to 60°C.

Energy Storage with Different PCMs. The predicted performance using numerical analysis for a Bi/Sn/In PCM used in place
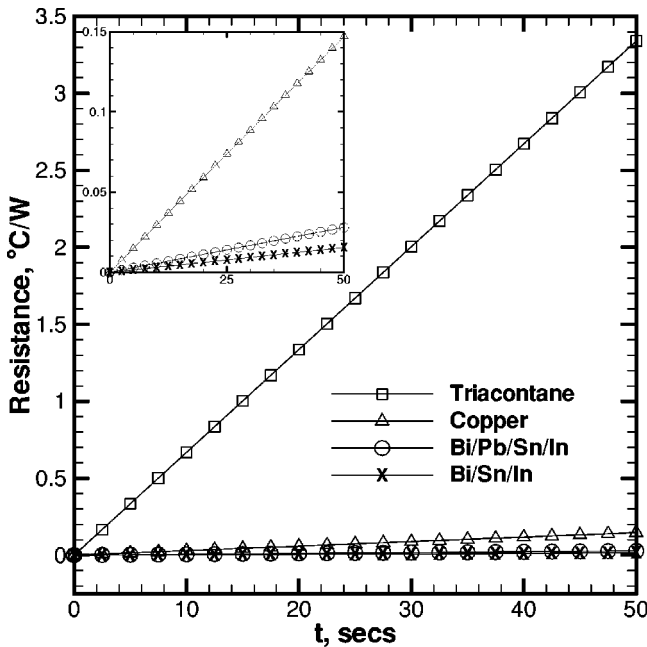

Fig. 3 Predicted thermal resistance as a function of time for the different materials considered, for a 300 W heat input for 50 s. In the inset, triacontane is omitted to distinguish between the much lower resistances of the other materials.
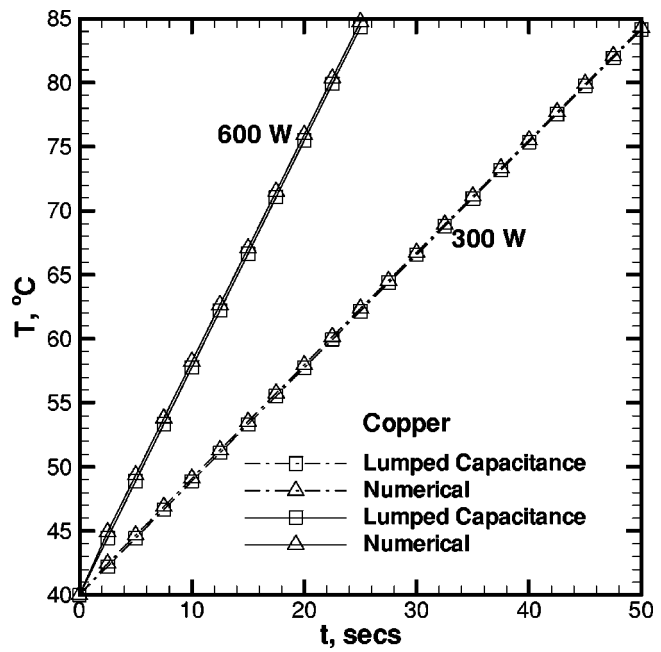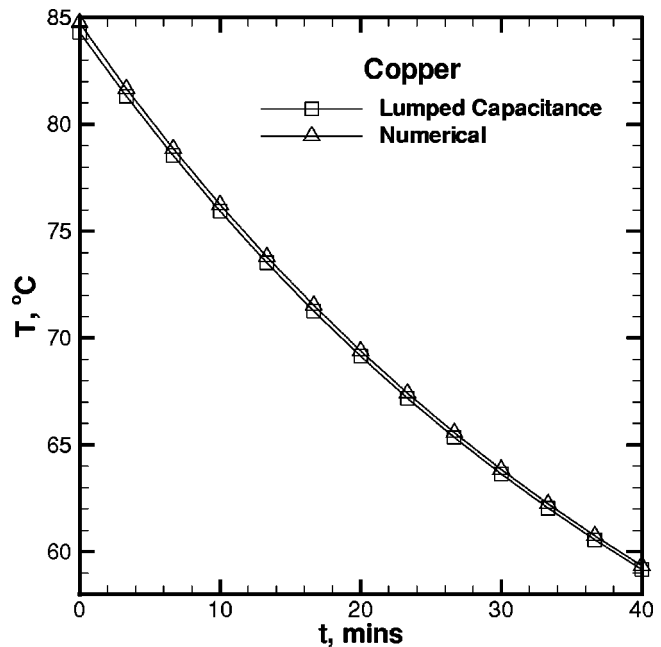

Fig. 5 Junction temperature during cooling of the copper heat sink as a function of time (after the end of the 600 W pulse input for 25 s)

Fig. 6 Temperature variation at the mid-height ($y=35$ mm) at different times for an input pulse of 300 W
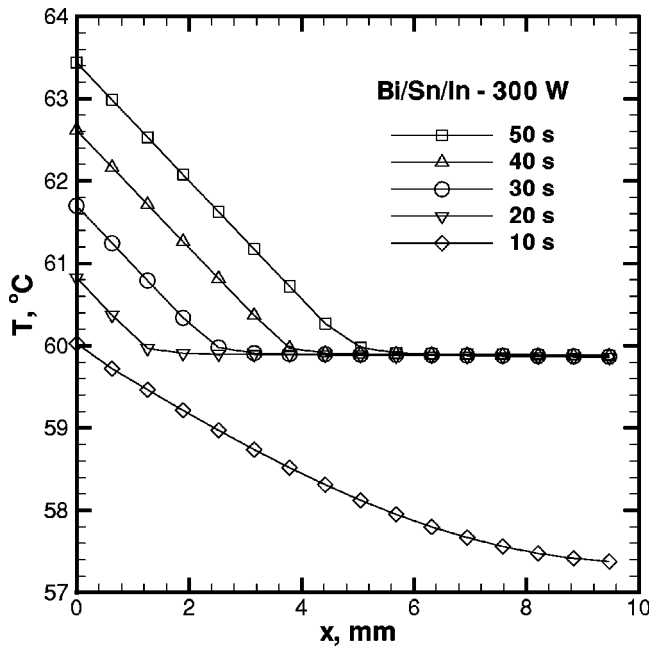

Fig. 7 Temperature variation at the mid-height ($y=35$ mm) at different times for an input pulse of 300 W

of the copper heat sink considered above is evaluated next. This PCM is a eutectic alloy with a melting temperature of 60°C. Since its properties were not available, a weighted average of the properties for the constituent elements was used (Table 1). This approach to property determination was successfully verified by also applying it to the Bi/Pb/Sn/In alloy, for which the property values are known. The predicted temperature variation across the mid-height of the domain ($y=35$ mm) is plotted for the PCM at different times in Fig. 6 for the lower of the two heat input pulse levels (300 W for 50 s). The PCM starts to melt approximately 10 s into the pulse (the approximate time to initiate phase change using Eq. (4) being 10.34 s), corresponding to the time it takes to heat up from its initial to its melting temperature. After this time, the melt region absorbs the heat input and increases in temperature, while the solid region remains at the melting temperature of 60°C.

The advantage of using the PCM is clear from a comparison of Figs. 6 and 4. The maximum temperature rise for a 300 W heat input with a copper heat sink was 84.3°C, whereas with the PCM, this maximum temperature rise is limited to 63.4°C. In addition, at the end of the input pulse, only the first 4.9 mm of the PCM layer has melted, pointing to the possibility of a significant reduction in the volume required for a PCM unit (from a 10 mm thickness for the copper heat sink to approximately 5 mm for the PCM unit).

Corresponding results from replacing the metallic alloy PCM with an organic PCM (triacontane) are shown in Fig. 7. Owing to the poor thermal conductivity of triacontane (even though its $\rho\Delta H$ product is comparable to that of Bi/Sn/In), unacceptably high temperatures result. Unless the effective thermal conductivity of the PCM is improved (with the use of metal foams or internal fins), it would not be a viable alternative for this application.

In order to improve the transient thermal performance of triacontane, an aluminum foam insert of porosity 0.8 was introduced into the PCM. Thermal equilibrium was assumed at the interface between the solid foam and the fluid matrix. Also the contact at the interface between the foam and the heat source was assumed to be perfect (no contact resistance). The thermal capacitance of the mixture is obtained using the relation

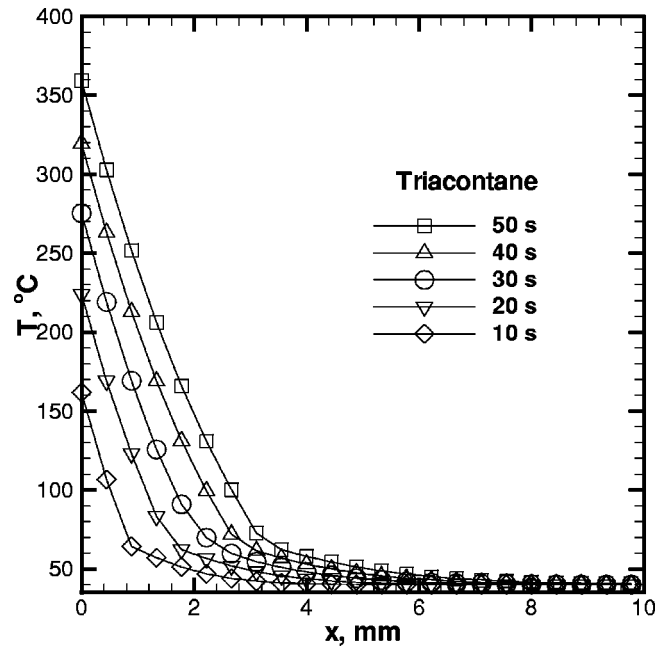$$(\rho C_p)_{\text{eff}} = \varepsilon(\rho C_p)_f + (1-\varepsilon)(\rho C_p)_{\text{PF}} \tag{6}$$

in which ε is the foam porosity. The effective thermal conductivity of the PCM-foam combination was obtained as [14]:

$$k_{\text{eff}} = \left(\left(\frac{2}{\sqrt{3}} \right) \left(\frac{r\left(\frac{b}{L_f}\right)}{k_f + \left(1 + \frac{b}{L_f}\right)\frac{(k_s - k_f)}{3}} + \frac{(1-r)\left(\frac{b}{L_f}\right)}{k_f + \left(\frac{2}{3}\right)\left(\frac{b}{L_f}\right)(k_s - k_f)} \right. \right.$$
$$\left. \left. + \frac{\frac{\sqrt{3}}{2} - \frac{b}{L_f}}{k_f + \left(\frac{4r}{3\sqrt{3}}\right)\left(\frac{b}{L_f}\right)(k_s - k_f)} \right) \right)^{-1} \tag{7}$$

in which b/L_f is given by the expression

$$\frac{b}{L_f} = \frac{-r + \sqrt{r^2 + \frac{2}{\sqrt{3}}(1-\varepsilon)\left(2 - r\left(1 + \frac{4}{\sqrt{3}}\right)\right)}}{\frac{2}{3}\left(2 - r\left(1 + \frac{4}{\sqrt{3}}\right)\right)}$$

The "area ratio" r is defined in [14] and for unit width of the fiber, it is the ratio of half-thickness of the fiber to half-thickness of bump. A value of $r=0.09$ was used as suggested in [14]; further discussion of this parameter choice is available in [14], in which good comparisons between numerical results and experimental measurements of thermal conductivity were obtained for this value of r.

The results from these simulations are shown in Fig. 8. By comparing with Fig. 7, the use of the metal foam is seen to be greatly beneficial to the performance of the unit. The temperature rise at the junction has reduced significantly, from 359.3°C to 74.4°C. Also more of the PCM has melted than in the case without the metal foam owing to the higher conductivity and smaller available PCM volume. The actual magnitudes of the predicted temperatures in this case, however, are a function of the assumptions involved in modeling the foam-PCM combination, and should be interpreted with care.
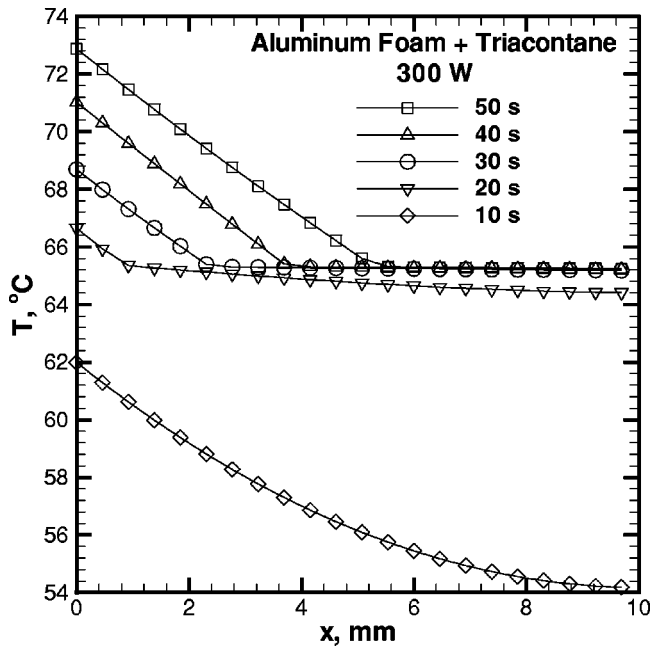
Fig. 8 Temperature variation at the mid-height ($y=35$ mm) at different times for an input pulse of 300 W

Fig. 10 Temperature variation at the mid-height ($y=35$ mm) for different pulses, at the end of the respective pulse input periods

Results corresponding to those discussed above are presented next for the higher heat input pulse considered (600 W for 25 s). Temperatures obtained with the Bi/Sn/In eutectic alloy are shown in Fig. 9. Compared to the lower heat input pulse considered in Fig. 6, the temperature rise at the junction is higher in Fig. 9. This would be expected from Eq. (T5), which, for a given thermal conductivity, density and latent heat, relates the temperature rise in the two cases according to:

$$\frac{(T_{\text{junction}} - T_{\text{melt}})_{\text{high}}}{(T_{\text{junction}} - T_{\text{melt}})_{\text{low}}} = \frac{(q''^2 t^*)_{\text{high}}}{(q''^2 t^*)_{\text{low}}} \quad (8)$$
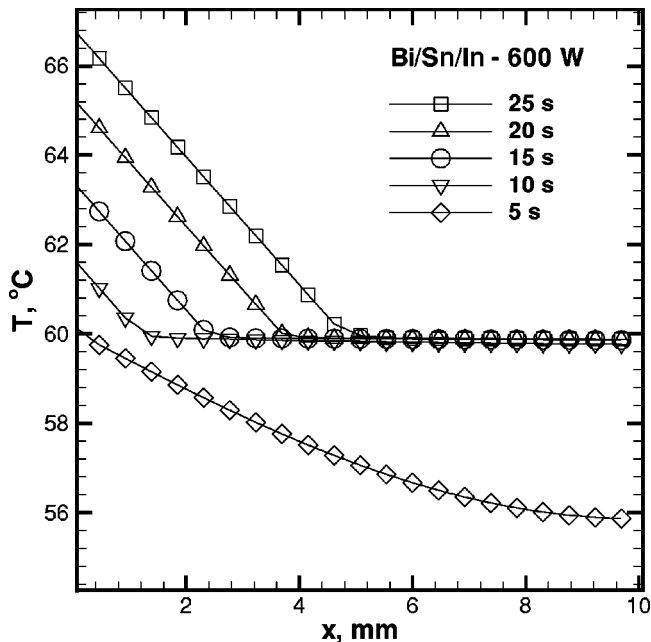

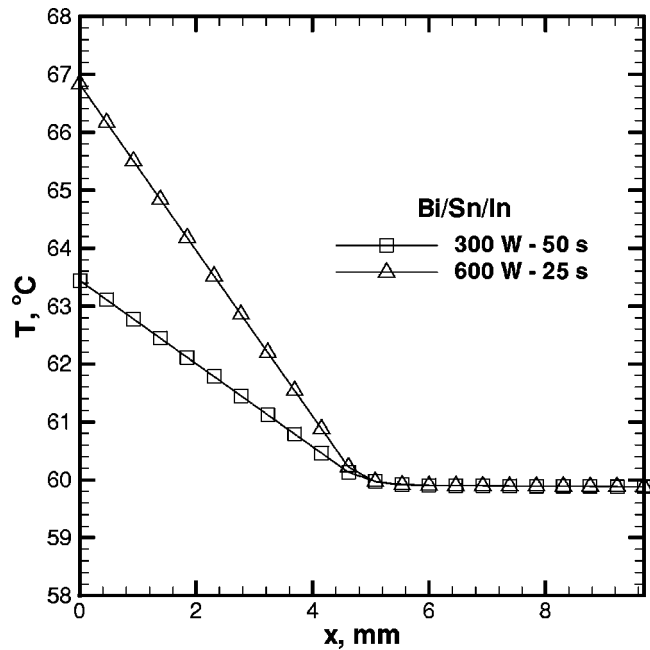**Fig. 9 Temperature variation at the mid-height ($y=35$ mm) at different times for an input pulse of 600 W**

The magnitude of this ratio is 2.0 for the two pulses considered. The implications of this equation can be clearly seen in Fig. 10. The junction temperature rise is 3.4°C for the 300 W input at the end of 50 s, while the temperature rise for the 600 W input at the end of 25 s is 6.8°C (greater by a factor of 2.0). Also, the ratio of the melted volumes is proportional to the ratio of energy inputs to the domain, and hence the amount of melted volume is the same for the chosen pulses because the ratio of energy input (in units of J) is unity. The front location predicted by the quasistationary solution (Eq. (T5)) is approximately 5 mm.

Figure 11 shows the temperature distribution at the mid-height ($y=35$ mm) for triacontane without and with the aluminum foam for the higher input pulse. It is again clear from the plots that introduction of the metal foam has an overwhelming effect on temperature suppression at the junction, while also causing an increase in the volume of PCM melted.

Resolidification. Resolidification (cooling) of the melted PCM after the end of the input energy pulse was also investigated, in an effort to determine the allowable frequency of repeated pulses. Results are shown in Fig. 12 for the resolidification process occurring at the end of the 50 s, 300 W input pulse, at which time the melt is allowed to cool by convection from the right wall. The left wall carrying the heat sources is considered to be perfectly insulated ($q''=0$) during the resolidification period, providing a conservative estimate of the resolidification time. For the Bi/Sn/In eutectic alloy PCM, Fig. 12 shows that the melted volume took approximately 65 minutes to resolidify. From Eq. (T7), it can be shown for small Biot number ($2/\text{Bi} \gg 1$) that

$$t \approx \frac{\rho \Delta H L}{h_\infty \Delta T} \approx \frac{\rho \Delta H}{h_\infty \Delta T} \left(\frac{V}{A} \right) \quad (9)$$

Therefore, the time for solidification is the ratio of the energy stored to the heat removal rate (J/m^3)/s. It should be noted from the above expression that thermal conductivity does not play a role in determining the solidification time. This is because the resistance to heat flow at the boundary between the PCM and the ambient (right wall) is higher than the resistance in the melt, and
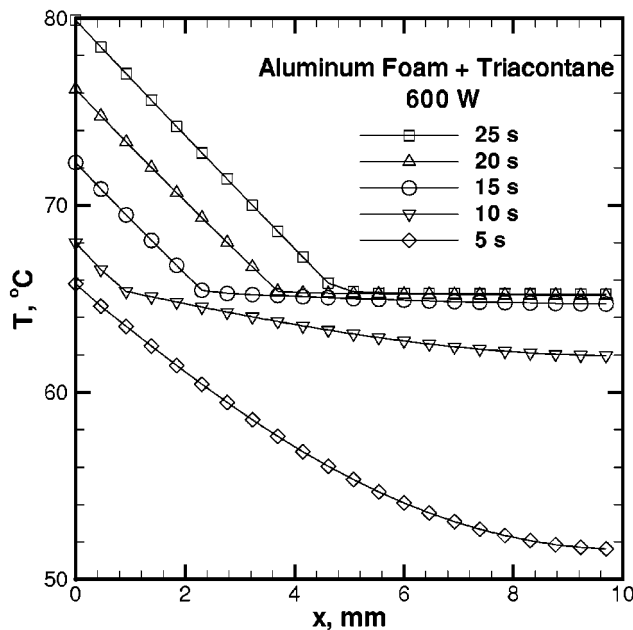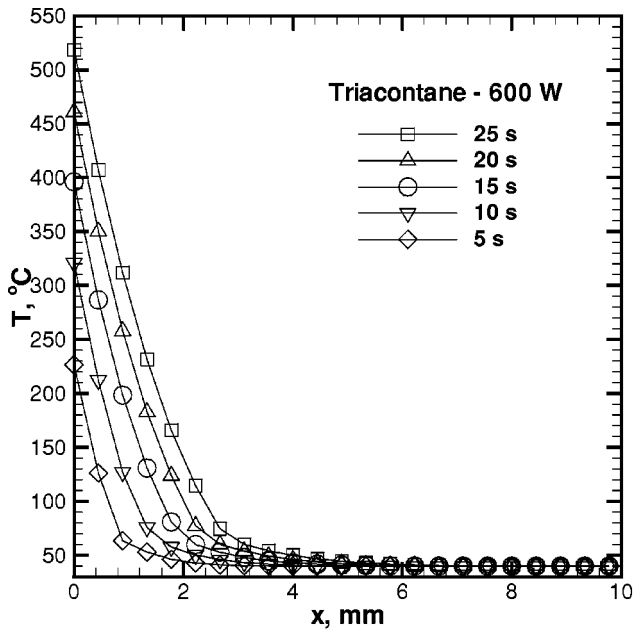
Triacontane - 600 W

☐	25 s
△	20 s
○	15 s
▽	10 s
◇	5 s

Fig. 12 **Predicted junction temperature as a function of time during cooling (melting and resolidification) for the Bi/Sn/In alloy PCM. The inset shows the detailed behavior at small times.**

Aluminum Foam + Triacontane 600 W

☐	25 s
△	20 s
○	15 s
▽	10 s
◇	5 s

Fig. 11 **Temperature variation at the mid-height ($y=35$ mm) at different times for triacontane for an input pulse of 600 W, with (a) PCM alone, and (b) PCM with aluminum foam**

the melt behaves as a "lumped" quantity. For h tending to infinity (i.e., a constant temperature condition), the heat removal rate is a maximum.

Performance of Different PCMs. The different materials considered in this study are compared in Figs. 13 and 14 for the lower and higher input pulses, respectively. Triacontane without foam is not included in this comparison since it results in unacceptably high temperatures. The temperature suppression at the junction is higher for the metallic alloys than for the aluminum foam impregnated with triacontane. A temperature rise from its melting temperature of approximately 9°C is seen for the foam with triacontane, while the temperature rise for the Bi/Sn/In alloy is approximately 3.4°C at the end of 50 s for a 300 W pulse input. At the end of the 600 W input ($t=25$ s), the temperature rise at the junction for the metal foam is 17°C, while for Bi/Sn/In alloy
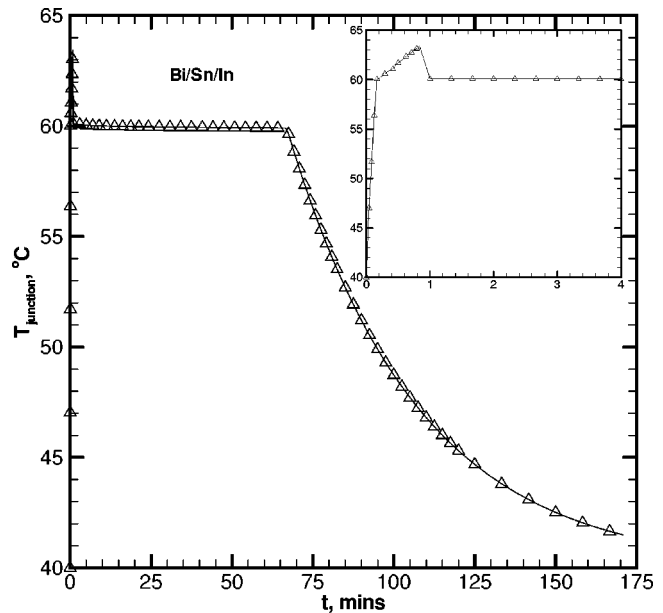
it is only 6.8°C. Both metallic alloys and the foam with triacontane yield significantly lower junction temperatures than a solid copper heat sink, for which junction temperatures of 84.3 and 84.7°C are obtained at the lower and higher input pulses, respectively.

The choice between a conventional heat sink and PCM-based heat sinks can be made using the expression

$$\frac{(T_{\text{junction}}(t) - T_{\text{melt}})_{\text{PCM}}}{(T_{\text{junction}}(t) - T_{\infty})_{\text{Metal}}} = q''L \frac{(\rho C_p)_{\text{Metal}}}{(k\rho\Delta H)_{\text{PCM}}} \left(1 - \frac{t_m}{t}\right) \quad (10)$$

300 W - 50 s

——	Copper
☐	Al Foam + Tricontane
△	Bi/Sn/In
○	Bi/Pb/Sn/In

Fig. 13 **Predicted temperature distribution at 50 s for a 300 W pulse input at the mid-height ($y=35$ mm) for copper heat sink, Bi/Pb/Sn/In and Bi/Sn/In alloys and organic PCM with a metal foam**
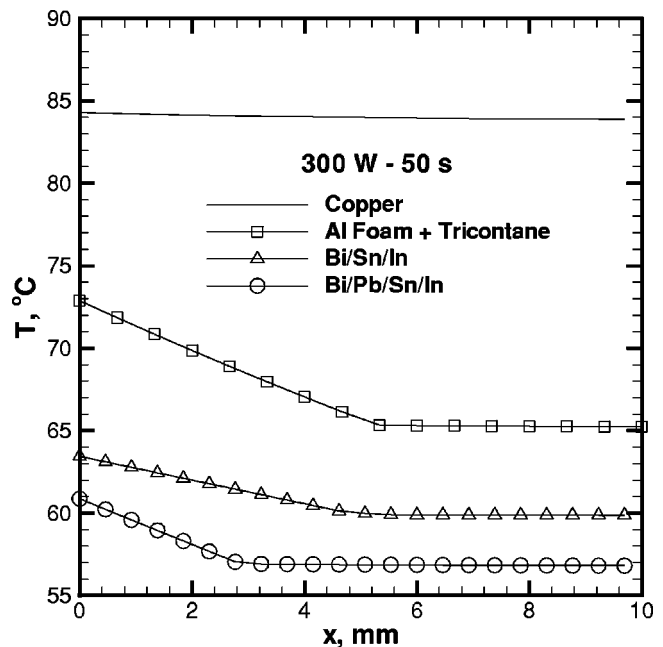
Fig. 14 **Predicted temperature distribution at 25 s for a 600 W pulse input at the mid-height ($y=35$ mm) for copper heat sink, Bi/Pb/Sn/In and Bi/Sn/In alloys and organic PCM with a metal foam**
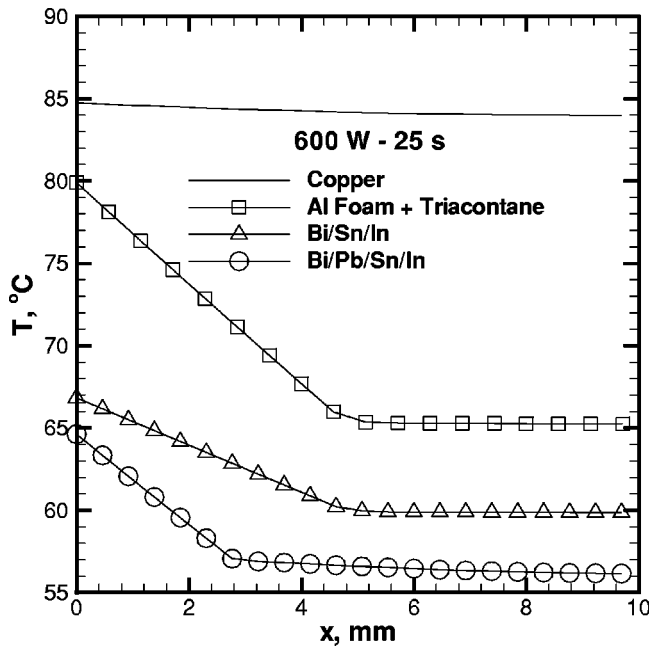
This expression results from Eq. (T5) and a linearized Eq. (T2). If the value of this ratio is less than 1, then the PCM unit will perform better than a conventional heat sink, in terms of suppression of junction temperature. Equation (10) suggests that although the volume savings achieved by employing a PCM can be estimated from the available latent heat energy ($\rho \Delta H$), the selection of the PCM itself must be based on the product of the thermal conductivity and this latent heat energy. For the 600 W input, the ratio for a Bi/Sn/In alloy PCM compared to a copper heat sink is 0.163; in contrast, for triacontane when compared to solid copper, this ratio is 36.7. This parameter provides for a clear design choice!

It may be noted as stated earlier that the quasi-stationary approximation is strictly valid when Ste=0. The linearized form shown in equation (4) results in an error of less than 2% in predicting the junction temperature, compared to the unlinearized equation (Eq. (T2)) when Fo<0.5 and Bi<0.1.

Design Methodology

For a specified heat input applied over a known period of time, the two desirable attributes of a cooling system are minimal volume and low junction temperatures. In using a phase change storage system, the volume chosen for the PCM unit should be such that all of the PCM just melts in the expected duration of the heat pulse. The desired melting point of the PCM itself is governed not only by the constraint on the junction temperature, but also on the desired temperature at the start of the succeeding pulse.

The first step in the design will involve a decision between a conventional (solid copper) heat sink and a PCM heat sink. For a chosen PCM, the effectiveness of the PCM can be compared to that of a copper (or aluminum) heat sink by employing Eq. (10). The decision can also be made alternatively using Eq. (5) for thermal resistance.

The approximate solutions presented in this paper can be used to design a PCM cooling unit with the desired performance. Consider a heat input of Q W applied over a surface of $y \times z$ m for $t1$ seconds. Let the PCM volume be $x \times y \times z$ m. The dimension of the PCM unit in the primary heat flow direction (x) is a vari-

able parameter. Let the ambient temperature be T_∞, and the required temperature in the PCM before exposure to a successive pulse ("restart") be T_{re}, desired to be within a period of t_2 seconds. Let the maximum allowable junction temperature be T_{max}. If multiple pulses are present, the performance of the PCM can be easily determined using Eq. (8). The design process would follow the steps below:

1. Since the restart temperature is T_{re} the melting point of the PCM should be greater than T_{re} for minimizing the volume; this determines the "first-cut" choice of the PCM to be used.

2. The junction temperature for the PCM chosen can be obtained using Eq. (T5). If $T_{junction}$ is greater than T_{max} then a different PCM should be chosen which results in a lower junction temperature.

3. From Eq. (T5), an approximate length for the domain can be calculated, $L = q''t_1 / (\rho \Delta H)$. The length calculated using this expression will always be greater than the optimal value since it does not account for the sensible heating of the PCM (time required to raise the PCM temperature to its melting point) and owing to shortcomings in the quasi-stationary approximation involved in the derivation of the approximate formula. Approximate estimates of volume savings derived from substituting PCMs for conventional metallic heat sinks can be obtained using the following expression

$$\frac{V_{PCM}}{V_{Metal}} \sim \frac{[\rho C_p (T_{junction} - T_\infty)]_{Metal}}{[\rho (C_p(T_{melt} - T_\infty) + \Delta H)]_{PCM}}$$

4. Using Eq. (T7) the approximate freezing time can be obtained, and the time for the process to reach the specified restarting temperature can be obtained from Eq. (T7).

Steps 1 through 4 should be repeated if the chosen PCM does not satisfy the requirements.

Conclusions

A transient thermal analysis was performed to compare the use of phase change materials and solid copper heat sinks for two different pulsed heat input levels. Easy-to-use expressions have been developed relating the material properties and geometric dimensions to enable quick design calculations for PCM units.

Four different PCMs (two metallic alloys, an organic material and an organic material imbedded inside a metal foam) were studied to explore possible trade-offs in their use. The computations show that an organic PCM without a thermal conductivity enhancer is a poor choice due to its very low thermal conductivity. The performance of the metallic PCMs and an organic PCM with a thermal conductivity enhancer can be comparable depending on the characteristics of the foam in question.

Although the thermal performance of the alloys is slightly better than that of the metal foam with the organic PCM, the density (package weight) of the alloy is an order of magnitude greater than that of the foam-PCM combination. This could be one important consideration in the choice of the cooling system. Other considerations may include the integrity of the foam under repeated thermal cycling, as well as the techniques used for bonding the foam to the heat spreader and thermal non-equilibrium [15,16] between the metal foam and the PCM.

Acknowledgment

Nomenclature

A = cross-sectional area, m^2
Bi = Biot number (hL k^{-1})
b = half-thickness of bump, m (Eq. (7))
C_p = Specific heat capacity, J kg^{-1} K^{-1}
E = thermal energy, J
Fo = Fourier number (αt L^{-2})
f_l = fraction of liquid
H = height of the domain, m
h = heat transfer coefficient, Wm^{-2} K^{-1}
k = thermal conductivity, Wm^{-1} K^{-1}
L = thickness (width) of the domain, m
L_f = half-length of the fiber, m (Eq. (7))
Q = heat input, W
q'' = heat flux (Q/A), Wm^{-2}
r = area ratio (Eq. (7))
S = interface location
Ste = Stefan number ($C_p \Delta T/\Delta H$)
T = temperature, °C
t = time, s
V = volume (AL), m^3

Greek Symbols

α = thermal diffusivity, m^2 s^{-1}
δ = melt depth, m
ε = porosity of the foam
η = temperature difference for phase change in Eq. (2), °C
ΔH = latent heat of the material, J kg^{-1}
ΔT = temperature difference, °C
ϕ = property
λ = roots of the transcendental equation (Eq. (3))
ρ = density, kg m^{-3}

Subscripts

eff = effective
f = fluid
j = junction
l = liquid
melt = melting
n = number
p = point

PF = porous foam
re = re-start
s = solid
∞ = ambient

Superscripts

qs = quasi-stationary
$\sim$ = vector

References

[1] Evans, A. G., He, M. Y., Hutchinson, J. W., and Shaw, M., 2001, "Temperature Distribution in Advanced Power Electronics Systems and the effect of Phase Change Materials on Temperature Suppression during Power Pulses," ASME J. Electron. Packag., **123**, pp. 211–217.

[2] Lu, T. J., 2000, "Thermal Management of High Power Electronics with Phase Change Cooling," Int. J. Heat Mass Transfer, **43**, pp. 2245–2256.

[3] Incropera, F. P., and DeWitt, D. P., 1998, *Fundamentals of Heat and Mass Transfer*, John Wiley & Sons, New York.

[4] Ishizuka, M., and Fukuoka, Y., 1991, "Development of a New High Density Package Cooling Technique Using Low Melting Point Alloys," Proceedings ASME/JSME Joint Thermal Engineering Conference, **2**, pp. 375–380.

[5] Pal, D., and Joshi, Y. K., 2001, "Melting in a Side Heated Tall Enclosure by a Uniformly Dissipating Heat Source," Int. J. Heat Mass Transfer, **44**, pp. 375–387.

[6] Krishnan, S., 2002, "Analysis of Phase Change Energy Storage Systems for Pulsed Power Dissipation," M.S.M.E. Thesis, Purdue University, West Lafayette, Indiana.

[7] Simpson, J. E., Garimella, S. V., and de Groh III, H. C., 2002, "An Experimental and Numerical Investigation of the Bridgman Growth of Succinonitrile," J. Thermophys. Heat Transfer, **16**, pp. 324–335.

[8] Ferziger, J. H., Peric, M., 1996, *Computational Methods for Fluid Dynamics*, Springer-Verlag, Berlin.

[9] Dantzig, J. A., 1989, "Modeling Liquid-Solid Phase Changes with Melt Convection," Int. J. Numer. Methods Eng., **28**, pp. 1769–1785.

[10] Alexiades, V., and Solomon, A. D., 1993, *Mathematical Modeling of Melting and Freezing Processes*, Hemisphere, Washington.

[11] Arpaci, V. S., 1972, *Conduction Heat Transfer*, Addison-Wesley, Massachusetts.

[12] Carslaw, H. S., and Jaeger, J. C., 1959, *Conduction of Heat in Solids*, Oxford, London.

[13] Solomon, A. D., 1980, "On the Melting Time of a Simple Body with a Convection Boundary Condition," Lett. Heat Mass Transfer, **7**, pp. 183–188.

[14] Calmidi, V. V., and Mahajan, R. L., 1999, "The Effective Thermal Conductivity of High Porosity Fibrous Metal Foams," ASME J. Heat Transfer, **121**, pp. 466–471.

[15] Krishnan, S., Murthy, J. Y., and Garimella, S. V., 2002, "A Two-temperature Model for the Analysis of Passive Thermal Control Systems for Electronics," *Proceedings of IMECE'02*, Paper No. IMECE2002-33335.

[16] Minkowycz, W. J., Haji-Sheikh, A., and Vafai, K., 1999, "On Departure from Local Thermal Equilibrium in Porous Media Due to Rapidly Changing Heat Source: the Sparrow Number," Int. J. Heat Mass Transfer, **42**, pp. 3373–3385.